Improving Railway Track Coverage with mmWave Bridges: A Measurement Campaign

Adrian Schumacher
Swisscom (Switzerland) Ltd. & EPFL
Bern, Switzerland
adrian.schumacher@swisscom.com

Nima Jamaly
Swisscom (Switzerland) Ltd.
Bern, Switzerland
nima.jamaly@swisscom.com

Ruben Merz
Swisscom (Switzerland) Ltd.
Bern, Switzerland
ruben.merz@swisscom.com

Andreas Burg
Ecole polytechnique fédérale de Lausanne (EPFL)
Lausanne, Switzerland
andreas.burg@epfl.ch

ABSTRACT

Bringing cellular capacity into modern trains is challenging because they act as Faraday cages. Building a radio frequency (RF) corridor along the railway tracks ensures a high signal-to-noise ratio and limits handovers. However, building such RF corridors is difficult because of the administrative burden of excessive formalities to obtain construction permissions and costly because of the sheer number of base stations. Our contribution in this paper is an unconventional solution of mmWave fronthauled low-power out-of-band repeater nodes deployed in short intervals on existing masts between high-power macro cell sites. The paper demonstrates the feasibility of the concept with an extensive measurement campaign on a commercial railway line. The benefit of using many low-power nodes with low-gain antennas compared to a baseline with only high-gain macro antennas is discussed, and the coverage improvement is evaluated. Based on the measurement results, a simple path loss model is calibrated. This model allows evaluation of the potential of the mmWave repeater architecture to increase the macro cell inter-site distance and reduce deployment costs.

CCS CONCEPTS

• **Networks** → **Mobile networks**; **Wireless access networks**; • **Hardware** → *Networking hardware*; *Wireless devices.*

KEYWORDS

5G, millimeter wave, bridge, repeater, railway, corridor

ACM Reference Format:
Adrian Schumacher, Nima Jamaly, Ruben Merz, and Andreas Burg. 2021. Improving Railway Track Coverage with mmWave Bridges: A Measurement Campaign. In *ACM SIGCOMM 2021 Workshop on 5G Measurements, Modeling, and Use Cases (5G-MeMU'21), August 23, 2021, Virtual Event, USA.* ACM, New York, NY, USA, 6 pages. https://doi.org/10.1145/3472771.3472774

Permission to make digital or hard copies of all or part of this work for personal or classroom use is granted without fee provided that copies are not made or distributed for profit or commercial advantage and that copies bear this notice and the full citation on the first page. Copyrights for components of this work owned by others than ACM must be honored. Abstracting with credit is permitted. To copy otherwise, or republish, to post on servers or to redistribute to lists, requires prior specific permission and/or a fee. Request permissions from permissions@acm.org.
5G-MeMU'21, August 23, 2021, Virtual Event, USA
© 2021 Association for Computing Machinery.
ACM ISBN 978-1-4503-8636-4/21/08…$15.00
https://doi.org/10.1145/3472771.3472774

1 INTRODUCTION

Train passengers stream music or video, surf the Internet with their mobile devices, or work with documents hosted in clouds. Thus, the demand for high-capacity mobile connectivity is constantly increasing. An inter-city double-deck train can carry around 1400 passengers during rush hour. With only 10 percent of the passengers using the cellular network at an average throughput of 5 Mbps [8, 11], a total capacity of 700 Mbps is required. Even with a 100 MHz cell bandwidth as available with 5G New Radio (NR), a significant spectral efficiency of >7 bit/s/Hz is required for such data rates, which in turn requires a high signal-to-noise ratio [10]. Unfortunately, modern railway carriages act as Faraday cages making it hard to use the cellular network inside. Several solutions to the attenuation problem exist, but most require installing onboard equipment, causing conflicts between the long life cycles of the railway industry and the fast evolution in telecommunications [4]. A first step to address the problem is to replace the train windows with laser-treated low-emissivity (Low-E) windows with a transmission loss close to regular windows while maintaining a high thermal insulation. The additional cost for laser-treated Low-E windows is a fraction of the cost for onboard repeaters. Additionally, cellular sites are built along the railway tracks to create a dedicated radio frequency (RF) corridor – a long linear cell. Multiple measurement campaigns have been conducted to study the characteristics [5, 6] and maximize the capacity provided into the train. Lately, a throughput of 1.2 Gbps has been achieved on a train traveling at around 140 km/h [14].

Building new macro sites implies a lengthy process requiring civil construction permissions from all involved landowners who provide the space for the macro sites and those affected by the optical fiber and power cable installation. A simplification of this process is to build all new macro sites for the RF corridor just next to the railway tracks on the property of the railway company. Unfortunately, the proximity to the tracks causes wide incidence angles for the electromagnetic waves between the macro antenna and the train windowpane. With the strict electromagnetic field (EMF) exposure regulations in Switzerland, the macro sites need an inter-site distance (ISD) of as low as 500 m to guarantee a sufficiently high signal power and capacity inside the train. With a cost of US$ 175,000 per macro site [3] and considering the length of the

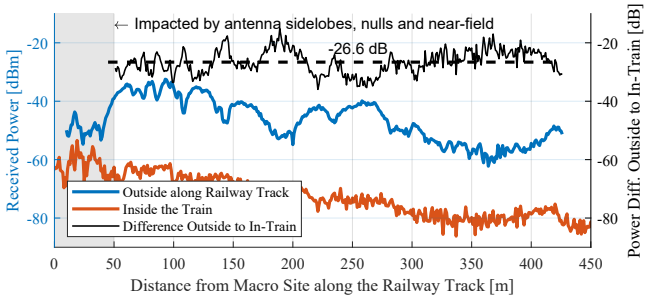

Figure 1: Measured signal power outside and inside the train and the resulting penetration attenuation.

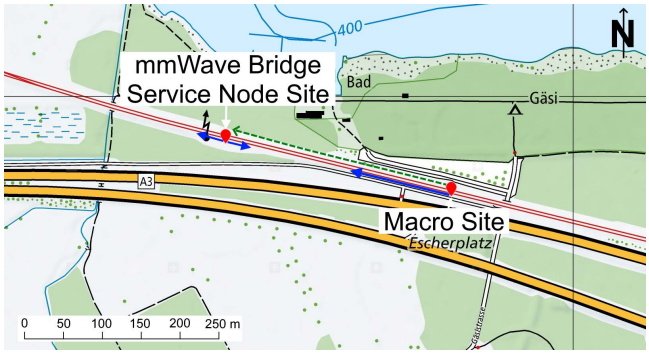

Figure 2: Antenna locations and their azimuth directions along the railway tracks (Source: Swisstopo [15]).

railway network with close to 1000 km of tracks in Switzerland to be equipped, the cost is prohibitive.

The motivation of this work is to find solutions to lower the number of RF corridor macro sites by increasing the ISD. Railway tracks for high speeds are often straight and must have curves with large radii. Masts for the railway overhead catenary wire exist every 50 m. Two conditions attenuate the link between the high-gain pencil beam macro antenna and a user equipment (UE) inside a train. First, the wide incidence angle to the train windowpane results in a narrow windowpane cross-section. Second, the catenary masts and the catenary overhead bars block the line-of-sight (LOS) between the macro antenna and the train windowpane. These angles and blockages cause an extra attenuation of 20 dB to 30 dB for the considered railway track section and used railway carriage as illustrated in Fig. 1.

The attenuation issue can be solved by installing additional lower-power antennas along the railway tracks to form a distributed antenna system (DAS) which maintains the received power levels inside the train at an increased macro ISD. The cell signals for the DAS can be fronthauled between the macro site and DAS nodes by an optical fiber. However, civil work constitutes 60-80 % of the total cost for antenna sites [3], and laying fiber to all nodes is costly; therefore, a wireless fronthaul can contribute to further savings as electrical power is often already available (or solar panels can be used). Finally, no permission for the antenna installation is required when the total effective radiated power (ERP) per antenna location is below 6 W, as it fulfills the condition for the EMF exposure limit of the general public [2, 13].

Our contribution is the proposal of a method to solve the railway RF corridor implementation problem using mmWave frequencies and low-power out-of-band repeater nodes. This mmWave bridge allows to increase the ISD of the dedicated macro sites and helps to lower the overall deployment cost. The use of mmWave frequencies for the fronthaul prevents interference to existing sub-6 GHz cells. Measurement results are presented to quantify the achievable ISD extension. The improvement in received power due to the presence of the mmWave bridge service nodes is analyzed.

The rest of this article is organized as follows: related work is summarized in Section 2. The cellular corridor trial installation and the measurement setup are described in Section 3. Section 4 explains how measurements have been performed and processed. The measurement results are presented and discussed in Section 5. Finally, Section 6 concludes this paper.
This work does not raise any ethical issues.

2 RELATED WORK

The deployment of a cellular trackside corridor for railways is described in [8]. An optical fiber ring distribution network connects base stations from a central location to remote antenna units (RAUs). An adaptation with fewer base stations is described in [4, 16]. Instead of installing one base station per RAU in the central station, a DAS is deployed that yields longer cells and fewer handovers. In [7], a further adaptation is presented that uses mmWave frequencies for the access link to the train. The authors in [1] extend the concepts mentioned above with the introduction of a dual-hop system. The trackside RAUs use mmWave frequencies to provide a high-capacity backhaul link to train antenna units operating as moving relay nodes. After the frequency conversion, a media converter is employed to create the access network, based, e.g., on WLAN, for the in-train network. Common to all these solutions is the required optical fiber network for supplying the radio signal to the trackside radio units. Due to the associated installation cost described in Section 1, cable or fiber-based solutions are not attractive. Furthermore, any installation onboard trains causes a conflict between the long life cycles of the railway industry for servicing or upgrading the onboard equipment and the fast evolution in telecommunications [4]. This conflict leads to a constant lag of the technology used onboard trains compared to what is available in the mobile network and UEs.

3 TRIAL INFRASTRUCTURE

A long linear cell along the railway track has been referred to as an RF corridor [4]. When such a corridor is implemented with pencil-beam antennas on the masts along and in the vicinity of the track, it is called an *antenna corridor* [6]. A railway track in the eastern part of Switzerland near lake Walensee [15] was selected to build and measure such an antenna corridor. Several macro sites with radio units (RU) and high-gain (25 dBi) pencil-beam antennas were built next to the two-lane railway track; see [6] for further details.

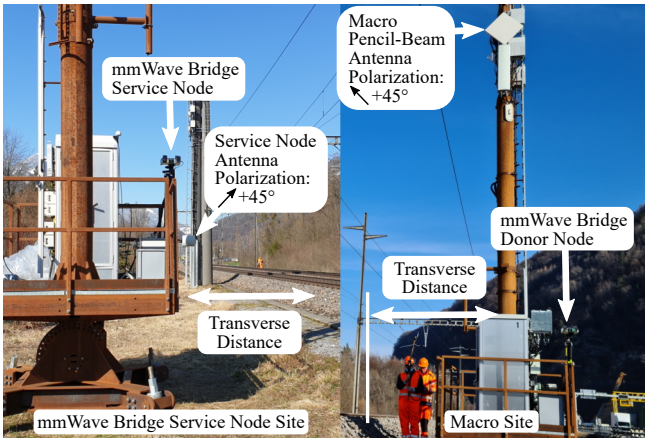

Figure 3: The macro antenna with the mmWave bridge donor node on the right, the service node on the left.

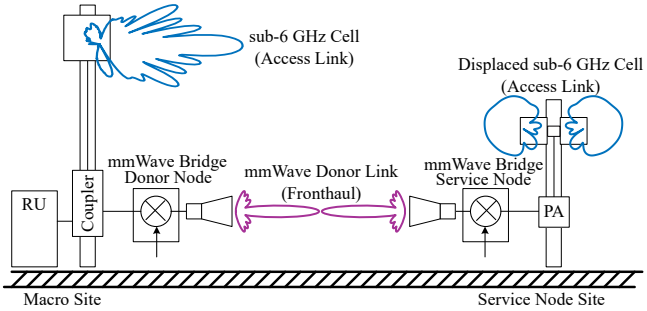

Figure 4: Schematic of the macro site and the mmWave bridge donor and service nodes.

3.1 Macro Site

The macro site used for the measurement campaign is labeled with "Macro Site" in Fig. 2 and hosts the NR RUs and macro antennas. The pencil-beam antenna for 3.6 GHz was installed at a height of 8.6 m above the railway track, with a transverse distance to the train windowpane of 3 m. The azimuth tuning of the main beam is aligned with the direction of the railway track towards west (blue arrow at "Macro Site" in Fig. 2), and the elevation tuning angle was 0°. For the measurements reported in this paper, the polarization +45° (up towards the railway track) was used; see the indication in Fig. 3.

A signal generator was installed to provide a continuous wave signal at 3.59 GHz fed to a 3 dB power divider. The first output was connected to a power amplifier for the macro site antenna. This branch gave a signal power of 24.2 dBm at the port of the pencil-beam antenna resulting in an ERP of 47.1 dBm. The second output of the power divider was connected to the mmWave bridge donor node input.

3.2 mmWave Bridge Installation

The mmWave bridge consists of a *donor node* and one or more *service nodes*. A directional coupler at the RF port of a macro cell RU feeds a fraction of the sub-6 GHz cell signal to the mmWave bridge donor node, where it is upconverted to a mmWave frequency and fronthauled to the mmWave bridge service node, see Fig. 4. The frequency downconversion in the service node translates the cell signal back to the original sub-6 GHz carrier frequency and the amplified cell signal is emitted by the antenna. The uplink operates in reverse direction. More details on the employed mmWave bridge and the prototype hardware can be found in [12]. For such a static installation, horn antennas with 25 dBi gain were used for the mmWave donor link on both nodes. Based on a test license from the Federal Office of Communications (OFCOM), the carrier frequency was configured to 39.75 GHz.

The mmWave bridge service node was installed on an existing platform at a distance of 292 m from the macro site, labeled "mmWave Bridge Service Node Site" in Fig. 2. At the mmWave bridge service node, the received and downconverted signal was connected to a power amplifier and then a 3 dB power divider connecting to the service antennas, see Fig. 4. Two 5.9 dBi gain Huber + Suhner antennas were mounted at the height of the train window in a back-to-back configuration, i.e., one antenna covering the railway track westwards and one covering the railway track eastwards at a transverse distance of 4.7 m to the train windowpane, see Fig. 3. The 3.6 GHz service antennas provided an ERP of 32.8 dBm and 32.5 dBm, respectively. Again, a polarization of +45° (up towards the railway track) was used. For the mmWave donor link, the Friis free space path loss suggests 113.7 dB loss. Based on the measured power levels, we obtained 116.3 dB.

4 MEASUREMENT METHODOLOGY

The trains used for the measurements were single-deck low-floor regional trains equipped with laser-treated Low-E windowpanes known as RF transparent windows.

For the measurements outside along the railway track, a Rohde & Schwarz FSH8 spectrum analyzer was used. The FSH8 was configured to conduct time domain measurements with a sweep time of 1 s. The resolution bandwidth (RBW) was manually set to 30 kHz. In order to continuously measure the signal, the FSH8 was set in spectrogram mode. During each sweep time, 631 power samples were captured and registered by the FSH8. A wideband dipole antenna from Huber + Suhner was connected to the FSH8 through a 2-meter cable of 1.8 dB loss. The antenna was held up at 2.5 m above ground, and the persons performing the measurements were walking at a constant speed on the cable duct along the railway track. Simultaneously, the Global Positioning System (GPS) location was recorded.

For the measurements inside the train, a Rohde & Schwarz FSW spectrum analyzer was used. The same dipole antenna was installed in a seat compartment on a tripod at 0.4 m from the windowpane at a height of 1.1 m above the floor. The FSW was configured to record the complex baseband signal with a sample rate of 10 kHz. Cable losses have been compensated in the measurements.

According to Lee's sampling criterion [9], fast fading effects have been mitigated by averaging the measured power samples in the linear domain over a distance of 40λ.

5 RESULTS AND DISCUSSION

Measurements of only the macro antenna have been conducted first to obtain a baseline scenario for comparison. Then, the mmWave bridge has been installed with the donor node at the macro site and the service node at a distance of 292 m. Accordingly, the foregoing measurements have been repeated with the mmWave bridge in operation in addition to the macro antenna as the second scenario. For each scenario, multiple train runs in both directions have been considered for measurement. As an indicator of uncertainty in our measurements, the average standard deviation was computed among all measurement runs. For the baseline scenario, a standard deviation of 3.1 dB is obtained and 2.6 dB for the scenario with the mmWave bridge.

5.1 Coverage for Macro Antenna (Baseline)

For the baseline scenario with only the macro antenna, the measured power levels inside the train are shown with red and orange lines in Fig. 5. The horizontal axis represents the distance along the railway track segment west of the macro site in Fig. 2. The measurements of four runs, two in opposite directions, have been averaged in linear domain and used to fit the power, modeled with the free space path loss and shown with a thick dark orange line. The resulting path loss with the calibration $L_{\mathrm{M,calib}} = 32.67$ dB is given according to

$$L_{\mathrm{M}}(d_{\mathrm{l}}) = \left(d_{\mathrm{l}}\frac{4\pi}{\lambda}\right)^2 \cdot L_{\mathrm{M,calib}} \quad \text{for } |d_{\mathrm{l}}| \geq d_{\mathrm{F}}, \tag{1}$$

where d_{l} represents the longitudinal distance on the railway track. The path loss is approximated as a constant for longitudinal distances below the Fraunhofer distance $d_{\mathrm{F}} = \frac{2D^2}{\lambda} = 17.2$ m defining the near-/far-field border of the pencil-beam antenna with D being the largest linear dimension. λ represents the wavelength of the carrier frequency. Note that the difference between the phase center of the macro antenna and the center of the railway carriage's middle windowpane in height and transversal distance is neglected, accepting an inaccuracy of 1 dB for $|d_{\mathrm{l}}| < d_{\mathrm{F}}$ in the studied configuration. The modeled power matches the measurements with a root mean squared error (RMSE) of 3.1 dB.

In Fig. 5, we note that for the first 200 m, there is a power difference of up to around 10 dB between the two railway tracks for the macro-only scenario. This difference can be explained by the two railway tracks having a transverse distance difference of 3.80 m, resulting in slightly different angles and windowpane cross-sections with the pencil-beam macro antenna. Due to the sidelobes in the antenna pattern, this results in a deviating antenna gain. Further, the blockage of the LOS by catenary masts is notably different for the railway track with a shorter transverse distance compared to the farther one. Finally, the measured power levels from the macro antenna are considerably higher between 50 m and 200 m than the free space path loss model suggests. These higher power levels can be explained with the antenna pattern and the two-ray ground reflection model.

5.2 mmWave Bridge Coverage Increase

The measured power with both the macro antenna *and* the mmWave bridge in operation is shown with green and blue lines in

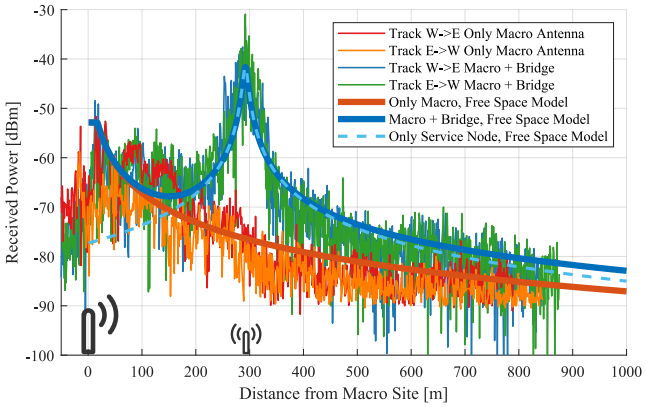

Figure 5: Measured signal power inside the train for only the macro antenna as a baseline and the macro antenna enhanced with the mmWave bridge at 292 m.

Fig. 5. Again, measurements from four runs, two in opposite directions, have been averaged in linear domain to fit the power with the free space path loss model for the macro antenna and service node combined, depicted with a thick blue line. The light blue dashed line represents the power only from the service node, based on the free space path loss model, adapted with the calibration $L_{\mathrm{S,calib}} = 18.75$ dB as

$$L_{\mathrm{S},n}(d_{\mathrm{l}}) = \left[d_{\mathrm{tv,S},n}^2 + \left(d_{\mathrm{l}} - d_{\mathrm{l,S},n}\right)^2\right]\left(\frac{4\pi}{\lambda}\right)^2 \cdot L_{\mathrm{S,calib}}. \tag{2}$$

Because the service node antennas are installed at the height of the railway carriage windowpane, the height difference can be neglected. However, the transversal distance of the nth service node antenna to the windowpane is represented with $d_{\mathrm{tv,S},n}$. The position of the nth service node along the longitudinal distance of the railway track is considered with $d_{\mathrm{l,S},n}$. The Fraunhofer distance is irrelevant due to the small dimension ($D = 0.25$ m) of the service node antenna. The RMSE of the modeled power compared with the measured power is 4.9 dB.

Comparing the two scenarios with and without mmWave bridge, Fig. 5 shows that the mmWave bridge service node provides a substantial increase in power starting at around 150 m. Even beyond 500 m up to 800 m, the service node lifts the power by 5-8 dB.

The difference between the high-gain macro antenna and the low-gain service node antennas can be analyzed by comparing the measured power levels outside and inside the railway carriage, see Fig. 6. The macro pencil-beam antenna with the 25 dBi gain creates a focused beam along the railway track, causing less scattering around the railway tracks to reflect power through the windowpanes into the carriage. This reduced scattering results in a carriage penetration gain of -26.6 dB (Fig. 1 with a 5° overshooting antenna) and -23.3 dB for the measurements with the mmWave bridge. The service antennas with a lower gain of 5.9 dBi therefore bring several advantages over a high-gain pencil beam antenna: first, the lower directivity allows for more power passing in LOS through the cross-section of the windowpane into the carriage; second, a reduced blockage of the LOS due to catenary masts and the height difference to the carriage windowpane; third, there are no sidelobes

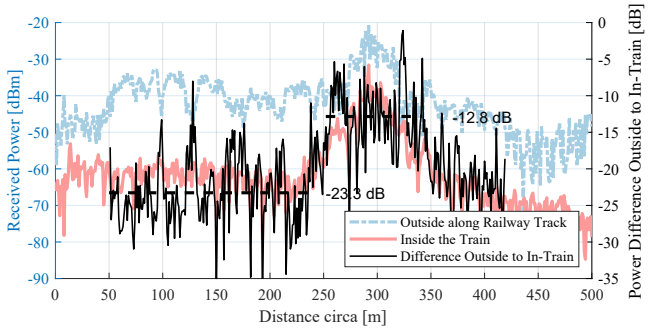

Figure 6: Signal power and difference for the macro and service node antennas outside and inside the train.

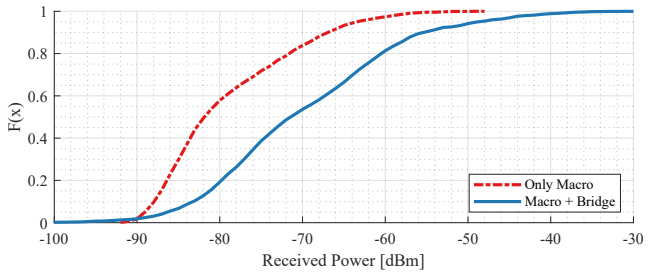

Figure 7: ECDF of all measurements taken in trains.

and nulls in the antenna pattern; fourth, they create a richer channel allowing for more reflections into the train resulting in a wagon penetration gain of -12.8 dB for the 50 m before and after the antenna; fifth, the antenna dimensions result in a significantly shorter near-field distance. The disadvantage of the lower gain is the more substantial power decrease in the longitudinal distance compared to the high-gain antenna, requiring shorter antenna installation intervals.

Finally, for each scenario, all measurement runs have been combined to calculate the empirical cumulative distribution function (ECDF) presented in Fig. 7. The additional mmWave bridge service node can increase the median power by 10.5 dB for the 1000 m railway track segment under study. NR throughput measurements have been done in the antenna corridor with only macro antennas. Based on these measurements, the linear regression for the throughput versus the reference signal received power (RSRP) gave a slope of 13.65 Mbps/dB for a 100 MHz NR cell. Hence, with an RSRP increase of 10.5 dB, an additional 143 Mbps can be achieved if the throughput is not saturating at the theoretical peak data rate.

While the presented measurement results are specific to the type of railway carriage, our further measurements suggest that these results are also applicable within 2-3 dB to other modern railway carriages. An impact on the signal attenuation from the mmWave bridge service node to the railway carriage is expected when two trains pass in opposite directions. However, at high velocities, the impact only lasts for a few seconds and does not lead to an outage.

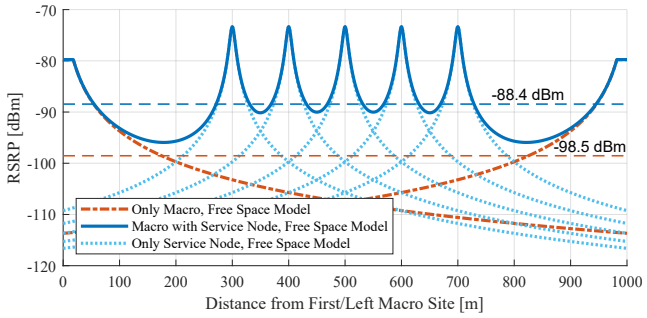

Figure 8: Example of a macro ISD of 1000 m with a transmit power of 600 W ERP and five mmWave bridge service nodes with a transmit power of 6 W ERP each. The average RSRP is shown with dashed lines.

5.3 Stretching the Macro ISD

The ultimate question we aim to address is the extension of the railway corridor macro ISD. To this end, a simple model is created according to (3) using the antennas' powers $P_{\mathrm{M}}^{\mathrm{RSTP}}$ for the macro antennas and $P_{\mathrm{S},n}^{\mathrm{RSTP}}$ for the N service node antennas, with the calibrated free space path loss models in (1) and (2), respectively. d_{ISD} denotes the macro ISD.

$$P_{\mathrm{UE}}^{\mathrm{RSRP}}(d_1) = \frac{P_{\mathrm{M}}^{\mathrm{RSTP}}}{L_{\mathrm{M}}(d_1)} + \frac{P_{\mathrm{M}}^{\mathrm{RSTP}}}{L_{\mathrm{M}}(d_{\mathrm{ISD}} - d_1)} + \sum_{n=1}^{N} \frac{P_{\mathrm{S},n}^{\mathrm{RSTP}}}{L_{\mathrm{S},n}(d_1)} \qquad (3)$$

For Long Term Evolution (LTE) and NR, it is common to know and compare power levels per subcarrier, represented by the RSRP. For this more intuitive interpretation, the power levels are offset by $10\log_{10}(1/3300)$ = -35.2 dB to reflect the difference between the composite power of a 100 MHz bandwidth cell and one subcarrier. In a typical example configuration for the numerical analysis here, the macro ISD is 1000 m with a macro antenna power of 600 W ERP, resulting in a reference signal transmit power (RSTP) of $P_{\mathrm{M}}^{\mathrm{RSTP}}$ = 181.8 mW (22.6 dBm). Five mmWave bridge service nodes have been placed with a 100 m inter-node spacing, centered between two macro sites. Each service node has an RSTP of $P_{\mathrm{S},n}^{\mathrm{RSTP}}$ = 1.82 mW (2.6 dBm), just at the EMF exposure limit of 6 W ERP for small-cells in the general public.

The numerical evaluation of (3) for the 5G NR RSRP inside the train is shown in Fig. 8. A scalar metric is used to compare different scenarios. If a train travels along the antenna corridor at a constant velocity, the measured power can be averaged over the distance. This resulting average RSRP is shown with dashed lines for the scenario with only the macro sites (orange lines) and the scenario with additional service nodes (blue lines), resulting in a 10.1 dB RSRP increase compared to only the macro antenna corridor.

Measurements have shown that 5G UEs can cope with power profiles as in Fig. 8 and variations of even 30 dB as frequently as every 50 m. Indeed, a UE inside a train moves by 28 mm per 5G NR slot of 0.5 ms at a train velocity of 200 km/h.

The above model in (3) can be used for various configurations. At first, a baseline configuration with only macro antennas every 500 m is assumed. This baseline is then compared to configurations

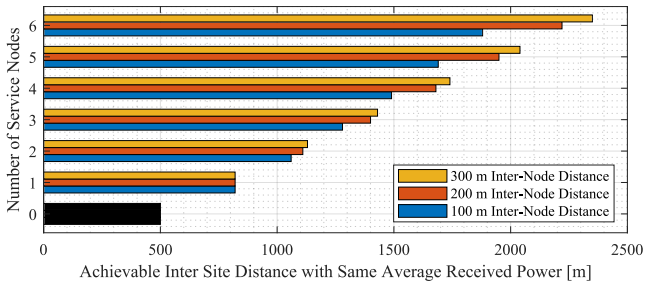

Figure 9: Numerical evaluation of average power in a train for a given number of mmWave bridge service nodes at a given inter-node distance.

with the macro antennas with a longer ISD and additional mmWave bridge service nodes installed in between. Because it is envisaged to install the mmWave bridge service nodes on the existing catenary masts, the available inter-node distance is limited to a multiple of 50 m. For our evaluation, inter-node distances of {100,200,300} m were chosen. A maximum number of six mmWave bridge service nodes are placed between the macro sites. Each macro site would feed a maximum of three mmWave bridge service nodes per side. By numerical evaluation of these configurations for a range of ISDs, the maximal macro ISD that can still provide at least the same average RSRP inside the train as the baseline configuration can be found as shown in Fig. 9.

With six mmWave bridge service nodes and an inter-node distance of 300 m, the same average RSRP can be achieved at a macro ISD of 2350 m as with a macro ISD of 500 m without using mmWave bridge service nodes. The farthest mmWave donor link would result in 1025 m which is still feasible under LOS, as the measurements in [12] have shown. Also, high-speed railway tracks are relatively straight, with large radii in curves, and the geological topography along the railway tracks often supports LOS for such distances.

6 CONCLUSION

A cellular antenna corridor is a solution to ensure a high signal-to-noise ratio and bring data capacity into trains. The installation of high-power macro sites in short intervals along the railway tracks is expensive. With out-of-band repeater nodes using mmWave frequencies for the fronthaul, multiple low-power service nodes can be installed between high-power macro sites. No interference is created on the existing network deployed on sub-6 GHz frequencies. The increased power levels allow stretching the macro site distance intervals, thereby lowering the cost. Measurements on a commercial railway line demonstrate the feasibility and show a median power increase of 10.5 dB for one service node with 14.6 dB less transmit power than the macro site. Calibrated path loss models were used to numerically evaluate several configurations and estimate the possible macro site distance increase. While this work supports a low-power distributed antenna system setup over a high-power antenna corridor, further applications such as fixed-wireless access to buildings are possible as presented in [12].

REFERENCES

[1] Pham Tien Dat, Atsushi Kanno, Naokatsu Yamamoto, and Testuya Kawanishi. 2015. WDM RoF-MMW and Linearly Located Distributed Antenna System for Future High-Speed Railway Communications. *IEEE Communications Magazine* 53, 10 (Oct. 2015), 86–94. https://doi.org/10.1109/MCOM.2015.7295468

[2] GSMA. 2016. *Improving Wireless Connectivity through Small Cell Deployment.* Research Report Booklet. GSMA. https://www.gsma.com/publicpolicy/wp-content/uploads/2016/12/GSMA_Small_Cell_Deployment_Booklet.pdf

[3] Weisi Guo and Tim O'Farrell. 2012. Capacity-Energy-Cost Tradeoff in Small Cell Networks. In *2012 IEEE 75th Vehicular Technology Conference (VTC Spring).* Yokohama, Japan, 1–5. https://doi.org/10.1109/VETECS.2012.6240225

[4] Nima Jamaly, Stefan Mauron, Ruben Merz, Adrian Schumacher, and Daniel Wenger. 2019. Delivering Gigabit Capacities to Passenger Trains: Tales from an Operator on the Road to 5G. *IEEE Communications Magazine* 57, 9 (Sept. 2019), 18–23. https://doi.org/10.1109/MCOM.2019.1800949

[5] Nima Jamaly, Damiano Scanferla, Carine Genoud, and Hugo Lehmann. 2018. Analysis and Measurement of Penetration Loss for Train Wagons with Coated vs Uncoated Windows. In *2018 12th European Conference on Antennas and Propagation (EuCAP).* London, UK, 610 (5 pp.). https://doi.org/10.1049/cp.2018.0969

[6] Nima Jamaly, Daniel Wenger, Reto Schoch, Matthias Rohrer, and Roger Jegerlehner. 2021. Measurement of Pathloss for Train Passengers in an Antenna Corridor. In *2021 15th European Conference on Antennas and Propagation (EuCAP).* Düsseldorf, Germany, 1–5.

[7] Atsushi Kanno, Pham Tien Dat, Naokatsu Yamamoto, and Tetsuya Kawanishi. 2018. Millimeter-Wave Radio-Over-Fiber Network for Linear Cell Systems. *Journal of Lightwave Technology* 36, 2 (Jan. 2018), 533–540. https://doi.org/10.1109/JLT.2017.2779744

[8] Bart Lannoo, Didier Colle, Mario Pickavet, and Piet Demeester. 2007. Radio-over-Fiber-Based Solution to Provide Broadband Internet Access to Train Passengers [Topics in Optical Communications]. *IEEE Communications Magazine* 45, 2 (Feb. 2007), 56–62. https://doi.org/10.1109/MCOM.2007.313395

[9] William C. Y. Lee and Yu-Shuan Yeh. 1974. On the Estimation of the Second-Order Statistics of Log Normal Fading in Mobile Radio Environment. *IEEE Transactions on Communications* 22, 6 (June 1974), 869–873. https://doi.org/10.1109/TCOM.1974.1092290

[10] Ruben Merz, Daniel Wenger, Damiano Scanferla, and Stefan Mauron. 2014. Performance of LTE in a High-Velocity Environment: A Measurement Study. In *Proceedings of the 4th Workshop on All Things Cellular: Operations, Applications, & Challenges.* ACM, New York, NY, USA, 47–52. https://doi.org/10.1145/2627585.2627589

[11] Darijo Raca, Dylan Leahy, Cormac J. Sreenan, and Jason J. Quinlan. 2020. Beyond Throughput, the next Generation: A 5G Dataset with Channel and Context Metrics. In *Proceedings of the 11th ACM Multimedia Systems Conference.* Association for Computing Machinery, New York, NY, USA, 303–308. https://doi.org/10.1145/3339825.3394938

[12] Adrian Schumacher, Ruben Merz, and Andreas Burg. 2021. Adding Indoor Capacity without Fiber Backhaul: An mmWave Bridge Prototype. *IEEE Communications Magazine* 59, 4 (2021), 6. https://doi.org/10.1109/MCOM.001.2000722

[13] Swiss Federal Council. 2019. SR 814.710 - Verordnung über den Schutz vor nichtionisierender Strahlung (NISV). https://www.fedlex.admin.ch/eli/cc/2000/38/de#annex_1/lvl_d1087e41/lvl_6/lvl_61

[14] Swisscom. 2020. Greater Bandwidth in Trains. https://www.swisscom.ch/en/about/news/2020/10/21-mehr-bandbreite-im-zug.html

[15] Swisstopo. 2021. Walensee Trial Railway Track. https://map.geo.admin.ch/?E=2726503&N=1220956&zoom=10

[16] Jiangzhou Wang, Huiling Zhu, and Nathan J. Gomes. 2012. Distributed Antenna Systems for Mobile Communications in High Speed Trains. *IEEE Journal on Selected Areas in Communications* 30, 4 (May 2012), 675–683. https://doi.org/10.1109/JSAC.2012.120502